International Journal of Engineering Research-Online
A Peer Reviewed International Journal
Articles available online http://www.ijoer.in; editorijoer@gmail.com

Vol.10, Issue.5, 2022
Sept-Oct

RESEARCH ARTICLE

ISSN: 2321-7758

SYNTHESIS, CHARACTERIZATION AND STUDY OF THE SURFACE PROPERTIES OF NANOPARTICULATED COBALT FERRITE

BADDEPUDI KAMALABABU
Lecturer in Chemistry
TRR Govt Degree College, Kandukur
Email: kamalababuchem@gmail.com
DOI: 10.33329/ijoer.10.5.1

ABSTRACT
This research focuses on a sol gel process for producing cobalt ferrite in the form of spherical nanoparticles. Furthermore, transmission electron microscopy, Fourier transform infrared spectroscopy, and electron diffraction are used to characterize the material's morphology and structure. Furthermore, the material's surface properties, including the point of zero charge (PZC), are investigated. The sol-gel method was used to synthesize cobalt ferrite ($CoFe_2O_4$), with cetyltrimethylammonium bromide (CTAB) serving as a surfactant. According to TEM, FTIR, and XRD, the nanoparticles had an average size of 10.5nm and a uniform distribution. According to the results of the analysis, the surfactant was successfully removed from the particle surface during the washing processes. Electron diffraction analysis also confirms the presence of a cobalt ferrite structure in the obtained oxide. The Davis, James, and Leckie (DJL) model was used to determine the number of surface sites, the relationship between surface charge density and pH, and the point of zero charge (PZC) of $CoFe_2O_4$.
Keywords: Nano ferrites, Synthesis, characterization, surface properties, Applications

INTRODUCTION

Nanostructured materials offer novel properties that are revolutionizing the technology of industrial applications. This is due to their physical and chemical properties, such as a higher surface area than that of massive solids, where a large fraction of the atoms occupies the edges of the nanoparticles. When the size of the nanoparticles is reduced, an increase in interfacial energy occurs due to defects, dislocations and imperfections in the reticular system [1], which leads to changes in the physical and mechanical properties of the materials, allowing them to adapt for certain uses in industry. Cobalt ferrite ($CoFe_2O_4$), is characterized by a high coercive field and a moderate saturation magnetization, with respect to other types of ferrites used in devices for data storage, catalysis, sensors, actuators as well as in medical applications such as delivery targeted medication, hyperthermia, cancer treatment, etc [2]. There are many conventional techniques for the preparation of metal oxide nanoparticles, including the sol-gel process, co-precipitation, evaporation, condensation, combustion etc., [3]. However, currently it is necessary to develop synthesis methods that are relatively simple and allow control of the size, morphology and dispersion of the particles. The success of its practical application is based on the ability to control the crystal size in the superparamagnetic (SPM) state and the monodomain boundaries. It is known that crystal size is related to the relative interdependence between nucleation and growth, steps that in turn can be strongly affected by reaction conditions [4].

Cobalt ferrite is a double oxide of iron(III) and cobalt(II), whose chemical formula is CoFeO. It is widely studied for its high magnetic anisotropy, moderate saturation magnetization, good chemical stability and mechanical hardness. Cobalt ferrite has an inverse spinel-type structure, that is, it is a face-centered cubic (FCC) network of oxygen anions, in which Fe (III) ions occupy all the tetrahedral holes and half of the octahedral ones, while the Co (II) ions occupy the other half of the octahedral spaces, as schematized in figure 1:

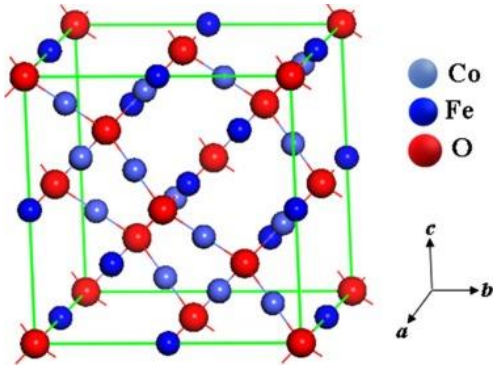

Figure 1. Scheme of the structure of cobalt 3 ferrite [5]

In gold extraction processes in mining companies [6], the filters in which the precious metal is captured have a working range influenced by the adsorption of other compounds from the solutions that make up the extraction mixture. Working conditions include a pH between 10-12 modulated by the addition of lime. Said lime is added in excess because it is intended to maintain the high pH to avoid producing HCN, which can be fatal. Said excess lime, necessary to maintain safe working conditions, causes particles of calcium hydroxides and carbonates to remain in the medium, which tend to be adsorbed in the filters that trap the gold. This generates a rise in the pressure necessary for pumping and reduces the working time of said filters. The use of ion exchange resins to reduce this concentration results in a decrease in the concentration of other cations (mainly univalent) in the solution, which, although present, do not influence the operational performance of the filters.

Therefore, because nanoparticles have a high area/volume (or area/mass) ratio, they have a large area to adsorb ions present in the medium and, as noted above, the surface charge of the cobalt ferrite It can be modified depending on the pH of the medium in which it is dispersed in such a way that, by adjusting the pH to a value found in the working conditions of mining extraction waters, it presents exchange capacities similar to those of the common exchange resins, using only 1/25 of the mass. However, due to the constant regeneration processes, they have 1/3 of the use time compared to conventional resins [7]. Even so, this negative effect is outweighed by the high exchange capacity (per unit of mass) that they present.

In the present study, the synthesis, characterization and magnetic properties of $CoFe_2O_4$ nanoparticles are reported, using CTAB as a surfactant in a simple reflux system varying the calcination temperature. This method offers the advantages of being relatively simple, low cost, and being an environmentally friendly alternative.

EXPERIMENTAL

The precursors Co $(NO_3)_3.6H_2O$ and Fe $(NO_3)_3.9H_2O$ were dissolved in distilled water at a concentration of 0.1M and 0.2M respectively and mixed with 2.0g of (CTAB) under constant stirring. KOH (25 ml) was added drop by drop into the solution until pH 11 was reached, forming a brown precipitate. The mixture was placed in a simple reflux system by adjusting the temperature to 180 °C and the reaction time to 6 h, then allowed to cool to room temperature. The product was washed with distilled water and ethanol and dried in an oven at 60 °C for 24 h. Finally, the sample was subjected to a 10-h heating ramp, in a muffle, varying the temperature from 200 °C to 800 °C in a N_2 atmosphere. For the following analyses, the colloid obtained was ultracentrifuged, the precipitated solid was washed and dried in an oven at 60°C for 4 days. The dried solid was stored in a desiccator for one more day.

Determination of the number of surface sites: To determine the number of surface sites, the addition method was carried out, in which 1 g of nanoparticles was added to a strongly basic solution, and the system was maintained with constant stirring for one hour, in which surface

equilibrium was reached. Subsequently, the expenditure of OH- ions was measured after the process.

Evaluation of the exchange capacity and regeneration: To evaluate the exchange capacity of the cobalt ferrite nanoparticles, standard calcium water of 660 ppm at pH ⍰ 8.3 was used, evaluating the [Ca^{2+}] with a standard 0.02M EDTA solution, until allowing a leak of 10 ppm. The final volume of standard water until leakage was quantified using appropriate glassware. For the regeneration step, 25 mL of 20% w/v NaCl solution was passed and the solid was washed 4 times with portions of 100 mL of deionized water each. If the chloride test (with $AgNO_3$ 0.017N) of the residual water was positive, a fifth washing was carried out until the chlorides were eliminated. The process was repeated 10 times to evaluate the decrease in exchange capacity with regeneration [9].

2.1 Characterization

Nanoparticulate cobalt ferrite was obtained by the method described in [4, 8]. Its structural and morphological characterization process included the techniques of transmission electron microscopy (TEM), Fourier transform infrared spectroscopy (FTIR) and electron diffraction (ED). The crystalline structure was analysed in a Bruker model D8 Focus polycrystalline samples Philips PW1250. For electron microscopy and electron diffraction, it was not It is not necessary to dry the sample or carry out any prior treatment for the analysis. It was enough to place a small amount of the colloid formed in the sample holder and let it dry in a desiccator. In the case of FTIR spectroscopy, the sample had to be precipitated with an electromagnet and washed until the chlorides present were eliminated. The morphology was observed using a FEI brand scanning electron microscope, model Quanta 200, and the average size was observed using a JEOL JEM 1220 transmission electron microscope. The TG and DSC analyses were developed using a TA thermal analyser model Q600. The surface area measurements from the N2 physisorption isotherms were carried out by the BET method on a MICROMERITICS device, model ASAP-2010.

Determination of PZC: To determine the PZC, the method described by DJL was put into practice. A potentiometric titration was performed on an aqueous solution at a set ionic strength with the nanoparticles, as well as a blank sample without them. This titration process required giving the system a commitment time to reach equilibrium, which could vary from 5 minutes to approximately half an hour, depending on how far one was from the surface neutrality condition. The 0.01 and 0.001 M potassium nitrate solutions were prepared by dilution of the more concentrated solution (0.1 M). Nitric acid was used to adjust the pH of the medium around 3 [10].

2.2 Particle size measurement

The average size of the nanoparticles was determined from the width at half height of the most intense peak of the diffraction pattern using the Scherrer equation [11]:

$$D = \frac{0.9\lambda}{\beta cos\theta} \quad \text{Eq...(1)}$$

where D is the average particle size, k is a shape function which has a value of 0.9, λ is the wavelength of the radiation (CuKα =0.154178 nm), β was determined from the integration of the half-width of the peak experimental (FWHM) and θ is the angle of incidence.

3. RESULTS AND DISCUSSION

Synthesis of cobalt ferrite: By ensuring the almost simultaneous precipitation of both ions, a solid known as green rust is formed. This has a lamellar double hydroxide structure, and is green in color due to the inevitable contamination with Fe(III) produced by the uncontrolled oxidation of part of the Fe(II) salts. Although this oxidation cannot be eliminated 100%, it can be minimized by working in a nitrogen atmosphere in special equipment known as a glovebox, which consists of an airtight box where the air inside can be removed using vacuum pumps and nitrogen introduced.

Because precipitation is carried out by both ions at pH between 7-8, it is ensured that both are incorporated into the solid structure, which will mean that in the subsequent thermal decomposition process, both are introduced

simultaneously to the ferrite, ensuring the production of a mixed oxide and not a mixture of the pure oxides of both.

Since the oxidation process of Fe(II) by O_2 is not controllable, an oxidizing agent must be sought that is capable of selectively converting Fe(II) to Fe(III), without oxidizing Co(II). The use of a mild oxidizing agent at room temperature would result in prolonged reaction times, which is not desirable. If the system is heated to a temperature lower than the boiling temperature of water, it is possible to increase the speed with which the oxidant acts, in addition to favouring the 'Ostwald Aging' process, by which the smallest particles that are formed, redissolve and reprecipitate on the larger ones, thus increasing the average particle size, but leading to a more homogeneous size distribution function. The time that must be used for this process to be carried out is several hours.

The oxidizing agent chosen was the nitrate ion. This is a mild oxidant at basic pH (11 was the pH at which ferrite was obtained), which decomposes in an anaerobic atmosphere to form nitrite [12].

The transformation between the green rust phase and the ferrite achieves the formation of homogeneous nanoparticles, sterically stabilized by the surfactant (CTAB) used in the process, as will be discussed in the following section.

The corresponding curves for TG and DSC analysis are shown in Figure 1. As the temperature increases, three significant weight loss regions are observed in the TG curve (red line). The first weight loss in the region of 25-200°C is associated with dehydration of the sample. The weight loss around 210 °C is attributed to the decomposition of organic species such as CTAB. The weight loss from 300 °C to 600 °C is related to the complete decomposition of the CTAB and the nitrate groups present in the sample.

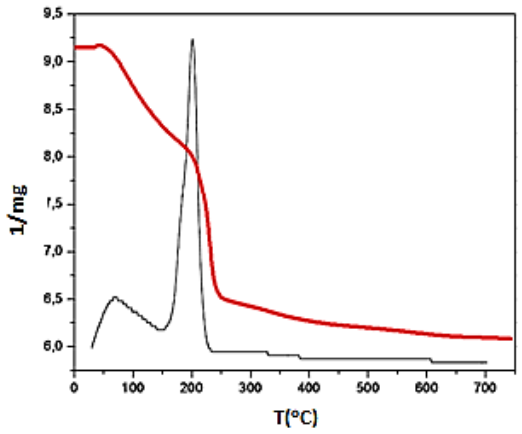

Figure 1. TG and DSC of the $CoFe_2O_4$ nanoparticles.

The DSC (black line) presents a highly intense exothermic peak around 210 ºC that corresponds to the decomposition process of nitrates and CTAB [13]. Figure 2 shows the X-ray diffraction patterns of $CoFe_2O_4$ nanoparticles prepared at 180 °C and thermally treated between 300 and 700 °C.

The diffraction patterns shown in Figure 2 are characteristic of the formation of the spinel structure, (220), (311), (222), (400), (422), (511), these peaks correspond to spinel cubic of $CoFe_2O_4$ ferrite (JPDS No. 22-1086) [12]. In this figure it can be seen that as the calcination temperature increases, the diffraction planes begin to intensify as a consequence of the crystallization of the material, with plane (311) being the one with the greatest intensity. The average size of the $CoFe_2O_4$ nanoparticles calculated from the half-width of the (311) diffraction peak using the Sherrer equation for the uncalcined sample was 9 nm, then this value was increased to 102 nm for the sample calcined at 800 °C.

Figure 3 shows the high-frequency absorption curves around 650-660 cm-1, which correspond to the intrinsic vibrations of the tetrahedral groups; in the range of 560-570 cm-1 the absorptions of the groups are found. octahedral. Low frequency absorptions are located at 370-380 cm-1 and are related to the presence of metal-oxygen ionic complexes [14]. Around 1381 cm-1, an intense absorption associated with the C-O bond of CTAB is observed [14]. This absorption suggests that the $CoFe_2O_4$ nanoparticles were successfully coated by the polymer.

The FTIR technique shows a peak at 598 cm-1 for the synthesized cobalt ferrite, corresponding to the band assigned to the Fe-O-Co vibration in cobalt ferrite [8,14] (which is located between 600-590 cm-1, in this case: 598 cm-1). No substantial difference is shown between this spectrum and that of a sample synthesized without surfactant, which shows that the CTAB used in the synthesis process is removed in the washing process.

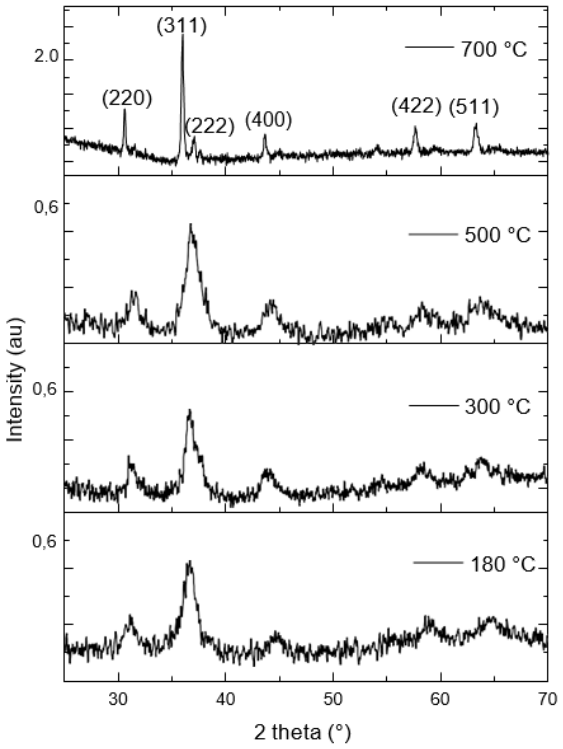

Figure 2. X-ray diffraction patterns of $CoFe_2O_4$ nanoparticles prepared at 180 °C and thermally treated between 300 and 700 °C.

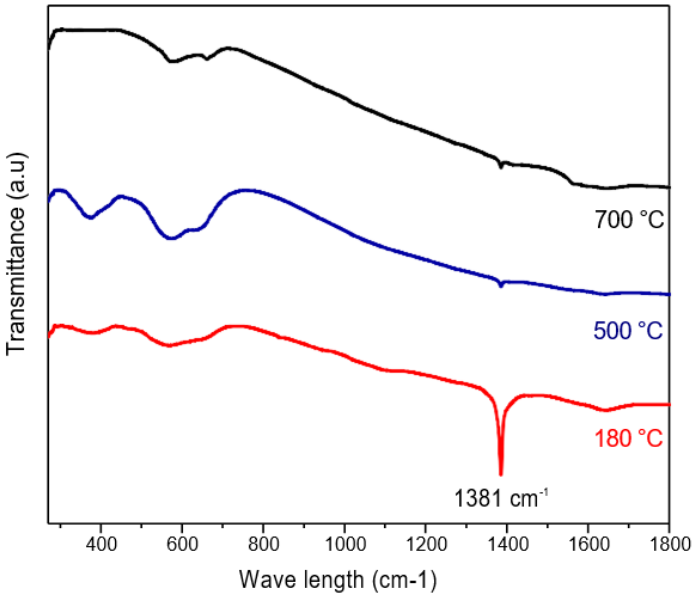

Figure 3. FT-IR spectra of $CoFe_2O_4$ nanoparticles thermally treated at 500 and 700°C.

The peaks corresponding to nitrate obtained from the FTIR spectrum, after washing, show that it is not completely removed from the particle. It should be noted that no thermal process was carried out after washing, which would ensure their elimination, but sintering reactions and particle growth could occur, especially due to the nanometric size at which we are working.

The removal of the surfactant after washing is a desirable process if surface property studies are to be carried out. In previous works [15], it has been shown that if another type of surfactant is used (such as sodium or potassium oleate), it is possible to obtain a selective surface complexation, and that by exhaustive washing with water, the surfactant is not eliminates. Although the particle size is smaller and the size distribution is more homogeneous, the fact of having the surfactant attached to the surface of the particle prevents the study of properties such as PZC or adsorption phenomena from reflecting the reality of the particle, since this limits the number of active surface sites, competing for them with the other ions present in the medium. Furthermore, the tails of the surfactant molecules attached to the surface of the particle hinder the ionic transfer process through the electrical double layer, increasing the times required to reach chemical equilibrium.

Figure 4 shows the MET micrographs 4(a) and SEM 4(b), 4(c) and 4(d), as well as the particle size distribution histograms. In the micrograph of Figure 4(a) you can see polydisperse $CoFe_2O_4$ nanoparticles, of irregular shape, with a size distribution between 4 and 14 nm, confirming the results obtained using XRD.

In Figures 4(b), 4(c) and 4(d) we can observe, using SEM, the surface of the nanoparticles studied, noting the presence of spongy and porous conglomerates, the small size of the particles facilitates the formation of conglomerates. In addition, atmospheric humidity contributes to this effect increasing. These conglomerates are formed due to the energetic and rapid generation of gases during the combustion process [16] and the Van der Wals forces between the particles.

In the micrograph of Figure 4(c), it is observed that the $CoFe_2O_4$ nanoparticles thermally treated at 600°C increase their average size distribution from 9 nm to 25 nm, while for the sample thermally treated at 800°C in Figure 4(d) the nanoparticles reach an average size of 100 nm. This figure shows the sintering of the material due to atomic diffusion between the contact surfaces of the nanoparticles.

The adsorption and desorption isotherms of a representative set of thermally treated $CoFe_2O_4$ nanoparticles are shown in Figure 5. From these isotherms it is verified that the sample treated at 400 °C is characteristic of materials with an intermediate porosity. At this temperature the material changes from micro to mesoporous, due to the emptying of the pores due to the loss of nitrate and hydroxyl groups and the decomposition of CTAB, as could be verified using XRD. The sample treated at 500°C presents a type II isotherm, characteristic of mesoporous materials with an H_2 hysteresis curve [16]. As the calcination temperature is increased from 500 °C to 600 °C the shape of the curve changes from H2 to H3 revealing a change in the pore structure. Curves of type H3 are usually assigned to particle conglomerates. At this temperature the pores are free of nitrate and hydroxyl groups and CTAB, this makes them larger than that of samples treated below 500°C. At temperatures above 700 °C, the material loses porosity and the isotherms do not present hysteresis, due to the increase in size, densification and subsequent agglomeration. of the nanoparticles [16], as could be seen in Figure 4(d). The textural characteristics of the $CoFe_2O_4$ nanoparticles are modified with thermal treatment, decreasing the number of intrinsic pores, which gradually translates into a reduction in the specific area as shown in figure 5.

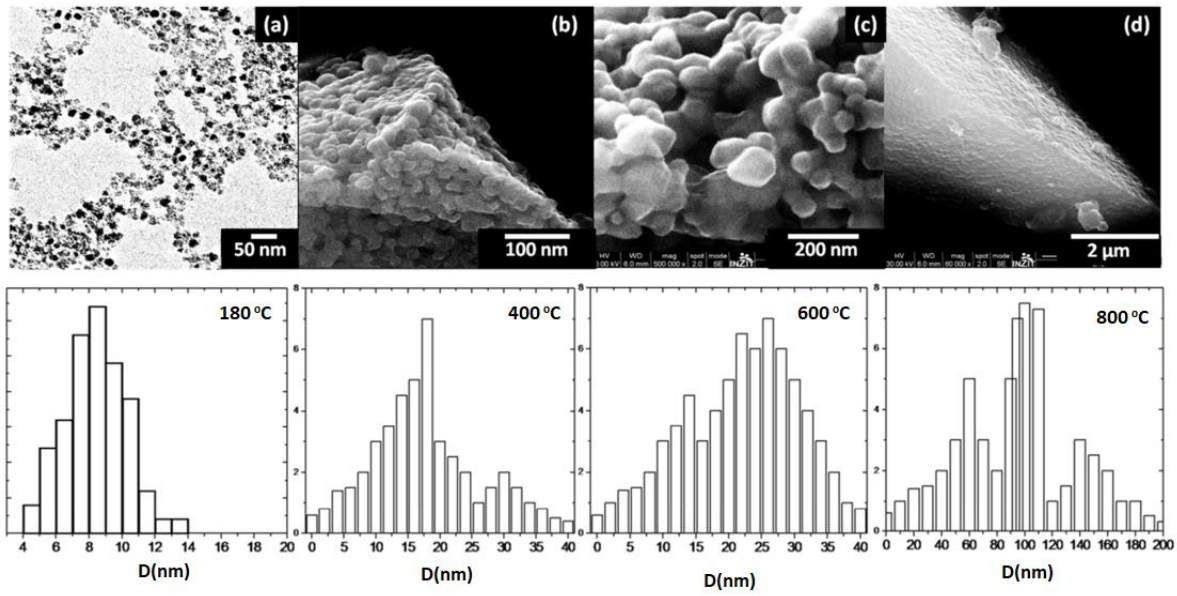

Figure 4. TEM and SEM of the $CoFe_2O_4$ nanoparticles prepared at 180 °C and thermally treated: (a) 200 °C, (b) 400 °C, (c) 600 °C and (d) 800 °C.

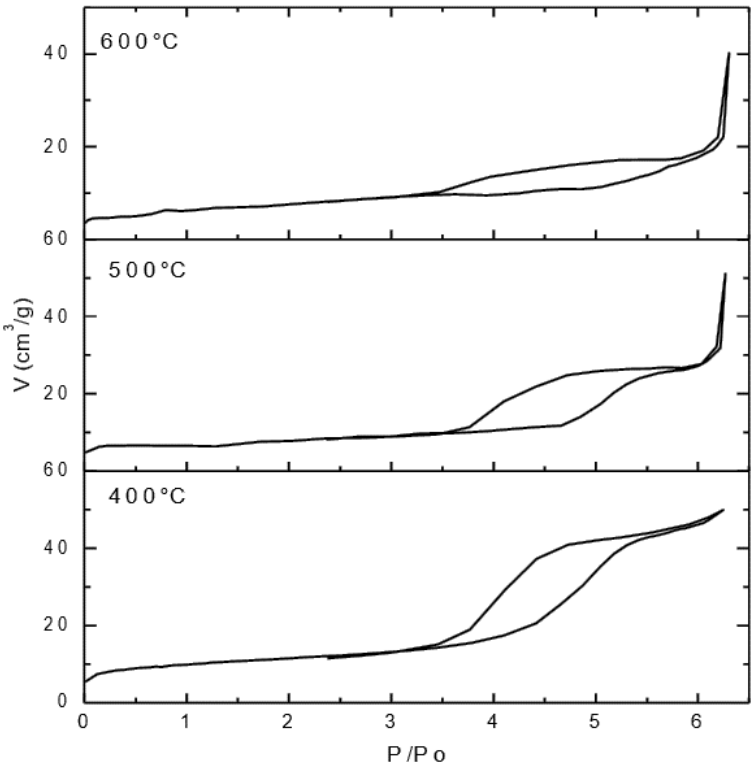

Figure 5. Adsorption isotherms of $CoFe_2O_4$ nanoparticles thermally treated between 400 and 600 °C.

The electron diffraction patterns show a face-centered cubic (FCC) crystal structure, which is in agreement with the structure of cobalt ferrite, which has an FCC arrangement of oxygen atoms in which, half of the octahedral holes are occupied by the Co(II) ion and the tetrahedral holes and the other half of the octahedral holes are occupied by the Fe(III) ion. The electron diffraction pattern, with the respective determination of the diffraction planes, is shown below [8, 17]:

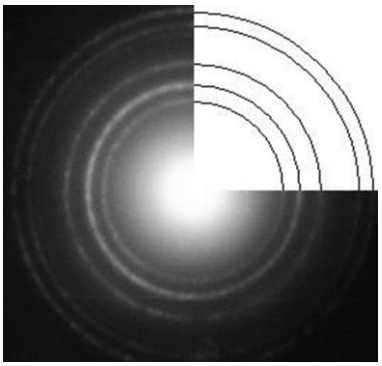

Figure 6: Electron diffraction pattern for the synthesized cobalt ferrite.

The interplanar distances calculated with the 'Diffraction' program are summarized, which is compared with the theoretical results for an FCC structure. The tabulated results confirm that the diffraction pattern corresponds to a face-centered cubic (FCC) crystal structure. The assignments of the Miller indices for each of the simulated concentric circles shown in Figure 6 are: [111], [200], [220], [311] and [222]. It should be noted that the electron diffraction technique was used instead of incident wave is much greater than the characteristic distance of the material. X-rays have wavelengths on the order of Å, while electrons accelerated with hundreds of kV have associated wavelengths 10-100 times smaller [18].

Determination of the PZC: As already mentioned in the previous chapters, to determine the PZC a potentiometric titration must be carried out. Said acid-base titration was carried out with 3 different ionic strengths using KNO_3. In all cases, the same amount of HNO_3 was added (giving a concentration of $4.0x10^{-4}$M) to bring the medium to an acidic pH for titration, and 1g of cobalt ferrite. The KOH concentration used was 0.08774 M (determined by colorimetric titration with potassium bi-phthalate).

With this graph it can be seen that the 3 curves intersect approximately at pH 7.3 at zero surface charge. Because there is no surface charge in the PZC, the influence of the electrolytes in the medium is zero at this point, which is why this cut-off value of the curves coincides with the PZC of the cobalt ferrite. In other works, values ranging from 6.5 to 8 [19] have been reported, depending on the method used for its measurement. The results of the surface charges fall within the values expected for similar oxides (for example magnetite: Fe_3O_4).

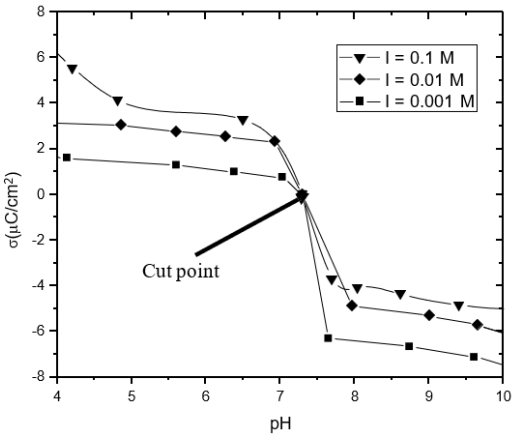

Figure 7: Surface charge of the particles (C/cm^2) vs pH at different ionic strengths (KNO_3)

Exchange Capacity: The ion exchange capacity, as defined above, is the amount of standard water ($[Ca^{+2}]$ = 660 ppm as $CaCO_3$, pH=8.3) that a material is capable of processing before producing a leak. of Ca^{+2} ions of 10 ppm expressed as $CaCO_3$. This is periodically monitored by taking a volume of 10 mL of the water leaving the resin and adding 1 mL of 0.001M EDTA standard solution. As long as $[Ca^{+2}]$ is below 10 ppm, the addition of eriochrome black T (NET) at pH 10 (controlled by the addition of NH_3-NH_4Cl buffer) the color of the solution remains blue. When changes in color are observed, the 10 mL samples are titrated with the standard EDTA solution until a leak of 10 ppm of Ca is obtained, expressed as $CaCO_3$. In the case of cobalt ferrite, the formation of specific bonds between the cations and the surface of the negatively charged particle (at pH > PZC), can significantly reduce the ion exchange capacity. Although metal oxides will not be harmed by swelling processes, coagulation by flocculation significantly decreases the ease with which ions can diffuse through the voids left in the flocs [20], decreasing the effective area that the particles possess for adsorption (this is because agglomeration causes said particles to come into contact and in said places in which they touch, the ions cannot adhere, even more so, if they are internal cavities produced by the contact of several particles). With the continuous regeneration processes, said coagulation becomes dominant and the drop in the exchange capacity is more

pronounced than in the case of resins, because coagulation is not 100% reversible, the effective exposed area constantly decreases. . However, a 25 times smaller amount of ferrite is capable of producing the same exchange capacity with only half the regenerations, making them about 10 times more adsorptive than common resins used in industrial softeners.

4. CONCLUSIONS

Cobalt ferrite nanoparticles were obtained by the sol gel process. The presence of cobalt ferrite was corroborated by Fourier transform infrared spectroscopy, its crystalline structure was identified as FCC and its preferential planes using the electron diffraction technique, and its spherical shape and medium size (10.5 ± 2.2 nm) by transmission electron microscopy

The study of the magnetic properties of the $CoFe_2O_4$ nanoparticles, in conjunction with the results of the structural characterization, allowed us to find correlations between the sizes of the nanoparticles, the coercivity values and the maximum magnetization, which would help determine which experimental conditions result suitable for obtaining nanoparticles with specific properties and being able to predict them based on the variation of the synthesis parameters. The point of zero charge (PZC) was determined by the DJL model in aqueous solution using KNO_3 as electrolyte, obtaining a value of 7.3. This result is within the range of the values determined for PZC in the literature. It was determined that the number of surface adsorption sites of cobalt ferrite by the addition method, using a KOH solution, was 9.3 sites/nm-2. This result also agrees with the reference values for the oxides published in other works. The exchange capacity of the ferrite was evaluated with the number of regenerations, determining that after 10 regenerating processes, the exchange capacity drops drastically. A superiority of this value was also shown at pH 10 compared to pH 8.3, due to the greater ionization of the surface groups of the cobalt ferrite.

References

[1]. Madkour, Loutfy. (2019). Properties of Nanostructured Materials (NSMs) and Physicochemical Properties of (NPs). 10.1007/978-3-030-21621-4_14.

[2]. Venturini, Janio & Mallmann Tonelli, Amanda & Wermuth, Tiago & Zampiva, Rúbia & Arcaro, Sabrina & Viegas, Alexandre & Bergmann, Carlos. (2019). Excess of Cations in the Sol-Gel Synthesis of Cobalt Ferrite ($CoFe_2O_4$): a Pathway to Switching the Inversion Degree of Spinels. Journal of Magnetism and Magnetic Materials. 482. 1-8. 10.1016/j.jmmm.2019.03.057.

[3]. Jeevanandam, Jaison & Barhoum, Ahmed & Chan, Yen San, Stephanie & Dufresne, Alain & Danquah, Michael. (2018). Review on nanoparticles and nanostructured materials: History, sources, toxicity, and regulations. Beilstein Journal of Nanotechnology. 9. 1050 - 1074. 10.3762/bjnano.9.98.

[4]. Kale, Swati & Somvanshi, Sandeep & Sarnaik, M. & More, S. & Shukla, S & Jadhav, K. M.. (2018). Enhancement in surface area and magnetization of CoFe2O4 nanoparticles for targeted drug delivery application. AIP Conference Proceedings. 1953. 030193. 10.1063/1.5032528.

[5]. Senthil, V.P. & Gajendiran, J. & Srinivasan, Gokul Raj & Shanmugavel, Thangavel & Kumar, G. & Reddy, Chandragiri. (2018). Study of structural and magnetic properties of Cobalt ferrite ($CoFe_2O_4$) nanostructures. Chemical Physics Letters. 695. 10.1016/j.cplett.2018.01.057.

[6]. Xie, Feng & Dreisinger, David. (2009). Use of ferricyanide for gold and silver cyanidation. Transactions of Nonferrous Metals Society of China. 19. 714-718. 10.1016/S1003-6326(08)60338-6.

[7]. Srivastava, Varsha & Kohout, Tomas & Sillanpää, Mika. (2016). Potential of cobalt ferrite nanoparticles ($CoFe_2O_4$) for remediation of hexavalent chromium from synthetic and printing press wastewater. Journal of Environmental Chemical Engineering. 4. 10.1016/j.jece.2016.06.002.

[8]. Suresh, Sagadevan & Podder, Jiban & Das, Isha. (2017). Synthesis and Characterization of Cobalt Ferrite ($CoFe_2O_4$) Nanoparticles Prepared by Hydrothermal Method. 10.1007/978-3-319-44890-9_14.

[9]. Ajroudi, Lilia & Villain, Sylvie & Madigou, Véronique & Thabet Mliki, Najeh & Leroux, Christine. (2010). Synthesis and microstructure of cobalt ferrite nanoparticles. Journal of Crystal Growth - J CRYST GROWTH. 312. 2465-2471. 10.1016/j.jcrysgro.2010.05.024.

[10]. Kumari, Nisha & Kour, Satvinder & Singh, Gurpreet & Kumar, Rajesh. (2020). A brief review on synthesis, properties and applications of ferrites. AIP Conference Proceedings. 2220. 020164. 10.1063/5.0001323.

[11]. Leitão Muniz, Francisco & Miranda, Marcus & Morilla-Santos, C. & Sasaki, José. (2016). The Scherrer equation and the dynamical theory of X-ray diffraction. Acta Crystallographica Section A Foundations and Advances. 72. 10.1107/S205327331600365X.

[12]. Farghali, Ahmed & Khedr, Mohamed & Khalek, Ahmed. (2007). Catalytic decomposition of carbondioxide over freshly reduced activated $CuFe_2O_4$ nano-crystals. Journal of Materials Processing Technology - J MATER PROCESS TECHNOL. 181. 81-87. 10.1016/j.jmatprotec.2006.03.053.

[13]. Chaturvedi, Shalini & Dave, Pragnesh. (2013). Review on Thermal Decomposition of Ammonium Nitrate. Journal of Energetic Materials. 31. 10.1080/07370652.2011.573523.

[14]. Mohamed hemeda, Osama. (2004). IR spectral studies of Co0.6Zn0.4MnxFe2−xO4 ferrites. Journal of Magnetism and Magnetic Materials. 281. 36–41. 10.1016/j.jmmm.2004.01.100.

[15]. Akmil-Başar, Canan & Karagunduz, Ahmet & Cakici, Avni & Keskinler, Bulent. (2004). Removal of surfactants by powdered activated carbon and microfiltration. Water research. 38. 2117-24. 10.1016/j.watres.2004.02.001.

[16]. Maranzana, Andrea & Tonachini, Glauco. (2011). Carbonaceous Nanoparticle Molecular Inception from Radical Addition and van der Waals Coagulation of Polycyclic Aromatic Hydrocarbon-Based Systems. A Theoretical Study. The Journal of Physical Chemistry C. 115. 10.1021/jp2010698.

[17]. Murugesan, Chelladurai & Murugesan, Perumal & Chandrasekaran, G.. (2014). Structural, dielectric and magnetic properties of cobalt ferrite prepared using auto combustion and ceramic route. Physica B: Condensed Matter. 448. 53-56. 10.1016/j.physb.2014.04.055.

[18]. Purnama, Budi & Wijayanta, Agung & Suharyana, Suharyana. (2018). Effect of calcination temperature on structural and magnetic properties in cobalt ferrite nano particles. Journal of King Saud University - Science. 31. 10.1016/j.jksus.2018.07.019.

[19]. Ibanez, Jorge & Hernandez-Esparza, Margarita & Doria-Serrano, Carmen & Fregoso-Infante, Arturo & Singh, Mono. (2008). The Point of Zero Charge of Oxides. 10.1007/978-0-387-49493-7_5.

[20]. Hosseini, Sayed Mohsen & Sohrabnejad, S. & Nabiyouni, Gholamreza & Jashni, Elham & Van der Bruggen, Bart & Ahmadi, A.. (2019). Magnetic cation exchange membrane incorporated with cobalt ferrite nanoparticles for chromium ions removal via electrodialysis. Journal of Membrane Science. 583. 10.1016/j.memsci.2019.04.069.